

000 054  
 001 055  
 002 056  
 003 057  
 004 058  
 005 059  
 006 060  
 007 061  
 008 062  
 009 063  
 010 064  
 011 065  
 012 066  
 013 067  
 014 068  
 015 069  
 016 070  
 017 071  
 018 072  
 019 073  
 020 074  
 021 075  
 022 076  
 023 077  
 024 078  
 025 079  
 026 080  
 027 081  
 028 082  
 029 083  
 030 084  
 031 085  
 032 086  
 033 087  
 034 088  
 035 089  
 036 090  
 037 091  
 038 092  
 039 093  
 040 094  
 041 095  
 042 096  
 043 097  
 044 098  
 045 099  
 046 100  
 047 101  
 048 102  
 049 103  
 050 104  
 051 105  
 052 106  
 053 107

## Supplementary File to “Multi-channel Weighted Nuclear Norm Minimization for Real Color Image Denoising”

Anonymous ICCV submission

Paper ID 572

In this supplementary file, we provide:

1. The proof of the Theorem 1 in the main paper.
2. More denoising results on the 24 high quality images from the Kodak PhotoCD dataset.
3. More visual comparisons of denoised images by different methods on the real noisy images of the dataset [1].
4. More visual comparisons of denoised images by different methods on the real noisy images of the dataset [2].

### 1. Proof of Theorem 1.

**Theorem 1.** Assume that the weights in  $w$  are in a non-descending order, the sequence  $\{\mathbf{X}_k\}$ ,  $\{\mathbf{Z}_k\}$ , and  $\{\mathbf{A}_k\}$  generated in Algorithm 1 satisfy:

$$(a) \lim_{k \rightarrow \infty} \|\mathbf{X}_{k+1} - \mathbf{Z}_{k+1}\|_F = 0; \quad (b) \lim_{k \rightarrow \infty} \|\mathbf{X}_{k+1} - \mathbf{X}_k\|_F = 0; \quad (c) \lim_{k \rightarrow \infty} \|\mathbf{Z}_{k+1} - \mathbf{Z}_k\|_F = 0. \quad (1)$$

*Proof.* 1. Firstly, we prove that the sequence  $\{\mathbf{A}_k\}$  generated by Algorithm 1 is upper bounded. Let  $\mathbf{X}_{k+1} + \rho_k^{-1} \mathbf{A}_k = \mathbf{U}_k \Sigma_k \mathbf{V}_k^\top$  be its singular value decomposition (SVD) [3] in the  $(k+1)$ -th iteration. According to Corollary 1 of [4], we can have the SVD of  $\mathbf{Z}_{k+1}$  as  $\mathbf{Z}_{k+1} = \mathbf{U}_k \hat{\Sigma}_k \mathbf{V}_k^\top = \mathbf{U}_k \mathcal{S}_{\frac{w}{\rho_k}}(\Sigma_k) \mathbf{V}_k^\top$ . Then we have

$$\|\mathbf{A}_{k+1}\|_F = \|\mathbf{A}_k + \rho_k(\mathbf{X}_{k+1} - \mathbf{Z}_{k+1})\|_F = \rho_k \|\rho_k^{-1} \mathbf{A}_k + \mathbf{X}_{k+1} - \mathbf{Z}_{k+1}\|_F \quad (2)$$

$$= \rho_k \|\mathbf{U}_k \Sigma_k \mathbf{V}_k^\top - \mathbf{U}_k \mathcal{S}_{\frac{w}{\rho_k}}(\Sigma_k) \mathbf{V}_k^\top\|_F = \rho_k \|\Sigma_k - \mathcal{S}_{\frac{w}{\rho_k}}(\Sigma_k)\|_F \quad (3)$$

$$= \rho_k \sqrt{\sum_i (\Sigma_k^{ii} - \mathcal{S}_{\frac{w}{\rho_k}}(\Sigma_k^{ii}))^2} \leq \rho_k \sqrt{\sum_i \left(\frac{w_i}{\rho_k}\right)^2} = \sqrt{\sum_i w_i^2}. \quad (4)$$

The inequality in the second last step can be proved as follows: given the diagonal matrix  $\Sigma_k$ , we define  $\Sigma_k^{ii}$  as the  $i$ -th element of  $\Sigma_k^{ii}$ . If  $\Sigma_k^{ii} \geq \frac{w_i}{\rho_k}$ , we have  $\mathcal{S}_{\frac{w}{\rho_k}}(\Sigma_k^{ii}) = \Sigma_k^{ii} - \frac{w_i}{\rho_k} \geq 0$ . If  $\Sigma_k^{ii} < \frac{w_i}{\rho_k}$ , we have  $\mathcal{S}_{\frac{w}{\rho_k}}(\Sigma_k^{ii}) = 0 < \Sigma_k^{ii} + \frac{w_i}{\rho_k}$ . After all, we have  $|\Sigma_k^{ii} - \mathcal{S}_{\frac{w}{\rho_k}}(\Sigma_k^{ii})| \leq \frac{w_i}{\rho_k}$  and hence the inequality holds true. Hence, the sequence  $\{\mathbf{A}_k\}$  is upper bounded.

2. Secondly, we prove that the sequence of Lagrangian function  $\{\mathcal{L}(\mathbf{X}_{k+1}, \mathbf{Z}_{k+1}, \mathbf{A}_k, \rho_k)\}$  is also upper bounded. Since the global optimal solution of  $\mathbf{X}$  and  $\mathbf{Z}$  in corresponding subproblems, we always have  $\mathcal{L}(\mathbf{X}_{k+1}, \mathbf{Z}_{k+1}, \mathbf{A}_k, \rho_k) \leq \mathcal{L}(\mathbf{X}_k, \mathbf{Z}_k, \mathbf{A}_k, \rho_k)$ . Based on the updating rule that  $\mathbf{A}_{k+1} = \mathbf{A}_k + \rho_k(\mathbf{X}_{k+1} - \mathbf{Z}_{k+1})$ , we have  $\mathcal{L}(\mathbf{X}_{k+1}, \mathbf{Z}_{k+1}, \mathbf{A}_{k+1}, \rho_{k+1}) = \mathcal{L}(\mathbf{X}_{k+1}, \mathbf{Z}_{k+1}, \mathbf{A}_k, \rho_k) + \langle \mathbf{A}_{k+1} - \mathbf{A}_k, \mathbf{X}_{k+1} - \mathbf{Z}_{k+1} \rangle + \frac{\rho_{k+1} - \rho_k}{2} \|\mathbf{X}_{k+1} - \mathbf{Z}_{k+1}\|_F^2 = \mathcal{L}(\mathbf{X}_{k+1}, \mathbf{Z}_{k+1}, \mathbf{A}_k, \rho_k) + \frac{\rho_{k+1} + \rho_k}{2\rho_k^2} \|\mathbf{A}_{k+1} - \mathbf{A}_k\|_F^2$ . Since the sequence  $\{\|\mathbf{A}_k\|_F\}$  is upper bounded, the sequence  $\{\|\mathbf{A}_{k+1} - \mathbf{A}_k\|_F\}$  is also upper bounded. Denote by  $a$  the upper bound of  $\{\|\mathbf{A}_{k+1} - \mathbf{A}_k\|_F\}$ , we have  $\mathcal{L}(\mathbf{X}_{k+1}, \mathbf{Z}_{k+1}, \mathbf{A}_{k+1}, \rho_{k+1}) \leq \mathcal{L}(\mathbf{X}_1, \mathbf{Z}_1, \mathbf{A}_0, \rho_0) + a \sum_{k=0}^{\infty} \frac{\rho_{k+1} + \rho_k}{2\rho_k^2} = \mathcal{L}(\mathbf{X}_1, \mathbf{Z}_1, \mathbf{A}_0, \rho_0) + a \sum_{k=0}^{\infty} \frac{\mu+1}{2\mu^k \rho_0} \leq \mathcal{L}(\mathbf{X}_1, \mathbf{Z}_1, \mathbf{A}_0, \rho_0) + \frac{a}{\rho_0} \sum_{k=0}^{\infty} \frac{1}{\mu^{k-1}}$ . The last inequality holds since  $\mu+1 < 2\mu$ . Since  $\sum_{k=0}^{\infty} \frac{1}{\mu^{k-1}} < \infty$ , the sequence of Lagrangian function  $\{\mathcal{L}(\mathbf{X}_{k+1}, \mathbf{Z}_{k+1}, \mathbf{A}_{k+1}, \rho_{k+1})\}$  is upper bound.

3. Thirdly, we prove that the sequences of  $\{\mathbf{X}_k\}$  and  $\{\mathbf{Z}_k\}$  are upper bounded. Since  $\|\mathbf{W}(\mathbf{Y} - \mathbf{X})\|_F^2 + \|\mathbf{Z}\|_{w,*} = \mathcal{L}(\mathbf{X}_k, \mathbf{Z}_k, \mathbf{A}_{k-1}, \rho_{k-1}) - \langle \mathbf{A}_k, \mathbf{X}_k - \mathbf{Z}_k \rangle - \frac{\rho_k}{2} \|\mathbf{X}_k - \mathbf{Z}_k\|_F^2 = \mathcal{L}(\mathbf{X}_k, \mathbf{Z}_k, \mathbf{A}_{k-1}, \rho_{k-1}) + \frac{1}{2\rho_k} (\|\mathbf{A}_{k-1}\|_F^2 - \|\mathbf{A}_k\|_F^2)$ . Thus  $\{\mathbf{W}(\mathbf{Y} - \mathbf{X}_k)\}$  and  $\{\mathbf{Z}_k\}$  are upper bounded, and hence the sequence  $\{\mathbf{X}_k\}$  is bounded by the Cauchy-Schwarz inequality

Table 1. PSNR(dB) results of different denoising methods on 24 natural images.

Image#	$\sigma_r = 5, \sigma_g = 30, \sigma_b = 15$								
	CBM3D	MLP	TNRD	NI	NC	WNNM-1	WNNM-2	WNNM-3	MC-WNNM
1	27.25	28.06	28.62	25.00	29.55	28.16	27.95	28.15	<b>30.20</b>
2	29.70	31.30	32.70	27.80	29.69	32.54	31.60	31.73	<b>34.04</b>
3	30.34	31.98	34.07	28.02	31.93	33.91	33.68	33.52	<b>35.55</b>
4	29.47	31.10	32.56	27.70	32.56	32.68	31.85	31.90	<b>34.06</b>
5	27.31	28.59	29.35	26.14	30.00	28.83	29.00	28.91	<b>30.05</b>
6	28.20	29.10	29.90	26.15	28.81	29.55	29.46	29.62	<b>31.64</b>
7	29.73	31.60	33.46	27.22	31.63	33.09	33.29	32.86	<b>34.24</b>
8	27.47	28.16	28.91	25.34	30.16	29.15	29.24	29.03	<b>29.91</b>
9	30.07	31.63	33.55	27.86	31.54	33.19	33.20	32.95	<b>34.53</b>
10	29.96	31.37	33.20	27.74	33.44	32.98	33.02	32.74	<b>34.38</b>
11	28.73	29.85	30.87	26.98	30.16	30.45	30.14	30.21	<b>32.10</b>
12	30.20	31.50	33.31	27.97	31.69	33.22	32.71	32.65	<b>34.64</b>
13	26.18	26.69	26.98	25.14	27.97	26.49	26.42	26.62	<b>28.30</b>
14	27.86	29.07	29.87	26.67	29.21	29.36	29.14	29.30	<b>31.18</b>
15	29.91	31.58	33.13	28.04	31.17	33.22	32.34	32.36	<b>34.27</b>
16	29.29	30.35	31.54	27.46	32.18	31.34	31.05	31.21	<b>33.72</b>
17	29.50	31.09	32.52	27.81	32.80	32.09	32.00	31.85	<b>33.61</b>
18	27.72	28.74	29.36	26.57	28.63	28.88	28.76	28.89	<b>30.56</b>
19	28.98	30.18	31.35	27.25	29.79	31.34	30.77	30.95	<b>33.10</b>
20	30.63	31.78	33.27	27.89	29.52	33.00	32.55	32.58	<b>34.18</b>
21	28.50	29.58	30.54	26.86	30.99	30.02	30.03	30.03	<b>31.69</b>
22	28.61	29.78	30.82	27.19	30.50	30.47	29.82	30.10	<b>32.08</b>
23	30.60	32.66	35.06	28.17	32.82	34.72	34.37	33.94	<b>35.16</b>
24	27.97	28.81	29.61	26.01	30.75	29.47	29.35	29.39	<b>30.93</b>
<b>Average</b>	28.92	30.19	31.44	27.04	30.73	31.17	30.91	30.89	<b>32.67</b>

and triangle inequality. We can obtain that  $\lim_{k \rightarrow \infty} \|\mathbf{X}_{k+1} - \mathbf{Z}_{k+1}\|_F = \lim_{k \rightarrow \infty} \rho_k^{-1} \|\mathbf{A}_{k+1} - \mathbf{A}_k\|_F = 0$  and the equation (a) is proved.

4. Then we can prove that  $\lim_{k \rightarrow \infty} \|\mathbf{X}_{k+1} - \mathbf{X}_k\|_F = \lim_{k \rightarrow \infty} \|(\mathbf{W}^\top \mathbf{W} + \frac{\rho_k}{2} \mathbf{I})^{-1} (\mathbf{W}^\top \mathbf{W} \mathbf{Y} - \mathbf{W}^\top \mathbf{W} \mathbf{Z}_k - \frac{1}{2} \mathbf{A}_k) - \rho_k^{-1} (\mathbf{A}_k - \mathbf{A}_{k-1})\|_F \leq \lim_{k \rightarrow \infty} \|(\mathbf{W}^\top \mathbf{W} + \frac{\rho_k}{2} \mathbf{I})^{-1} (\mathbf{W}^\top \mathbf{W} \mathbf{Y} - \mathbf{W}^\top \mathbf{W} \mathbf{Z}_k - \frac{1}{2} \mathbf{A}_k)\|_F + \rho_k^{-1} \|\mathbf{A}_k - \mathbf{A}_{k-1}\|_F = 0$  and hence (b) is proved.

5. Finally, (c) can be proved by checking that  $\lim_{k \rightarrow \infty} \|\mathbf{Z}_{k+1} - \mathbf{Z}_k\|_F = \lim_{k \rightarrow \infty} \|\mathbf{X}_k + \rho_k^{-1} \mathbf{A}_{k-1} - \mathbf{Z}_k + \mathbf{X}_{k+1} - \mathbf{X}_k + \rho_k^{-1} \mathbf{A}_{k-1} + \rho_k^{-1} \mathbf{A}_k - \rho_k^{-1} \mathbf{A}_{k+1}\|_F \leq \lim_{k \rightarrow \infty} \|\Sigma_{k-1} - \mathcal{S}_{w/\rho_{k-1}}(\Sigma_{k-1})\|_F + \|\mathbf{X}_{k+1} - \mathbf{X}_k\|_F + \rho_k^{-1} \|\mathbf{A}_{k-1} + \mathbf{A}_{k+1} - \mathbf{A}_k\|_F = 0$ , where  $\mathbf{U}_{k-1} \Sigma_{k-1} \mathbf{V}_{k-1}^\top$  is the SVD of the matrix  $\mathbf{X}_k + \rho_{k-1} \mathbf{A}_{k-1}$ .  $\square$

## 2. More denoising results on the 24 high quality images from the Kodak PhotoCD dataset

In the main paper, we have given the PSNR results of the competing methods on the 24 high quality images from the Kodak PhotoCD dataset when the standard deviations of the additive white Gaussian noise (AWGN) are  $\sigma_r = 40, \sigma_g = 20, \sigma_b = 30$  for R, G, B channels, respectively. Here we provide more denoising results on this dataset. In Tables ??-??, we give more PSNR results on these images when the noise standard deviations are  $\sigma_r = 5, \sigma_g = 30, \sigma_b = 15$  in Table 1 and  $\sigma_r = 30, \sigma_g = 10, \sigma_b = 50$  in Table 2, respectively. In Figures 5-??, we give the visual comparisons of the denoised images by different methods.

216

217

218

219

220

221

222

223

224

225

226

227

228

229

230

231

232

233

234

235

236

237

238

239

240

241

242

243

244

245

246

247

248

249

250

251

252

253

254

255

256

257

258

259

260

261

262

263

264

265

266

267

268

269

270

271

272

273

274

275

276

277

278

279

280

281

282

283

284

285

286

287

288

289

290

291

292

293

294

295

296

297

298

299

300

301

302

303

304

305

306

307

308

309

310

311

312

313

314

315

316

317

318

319

320

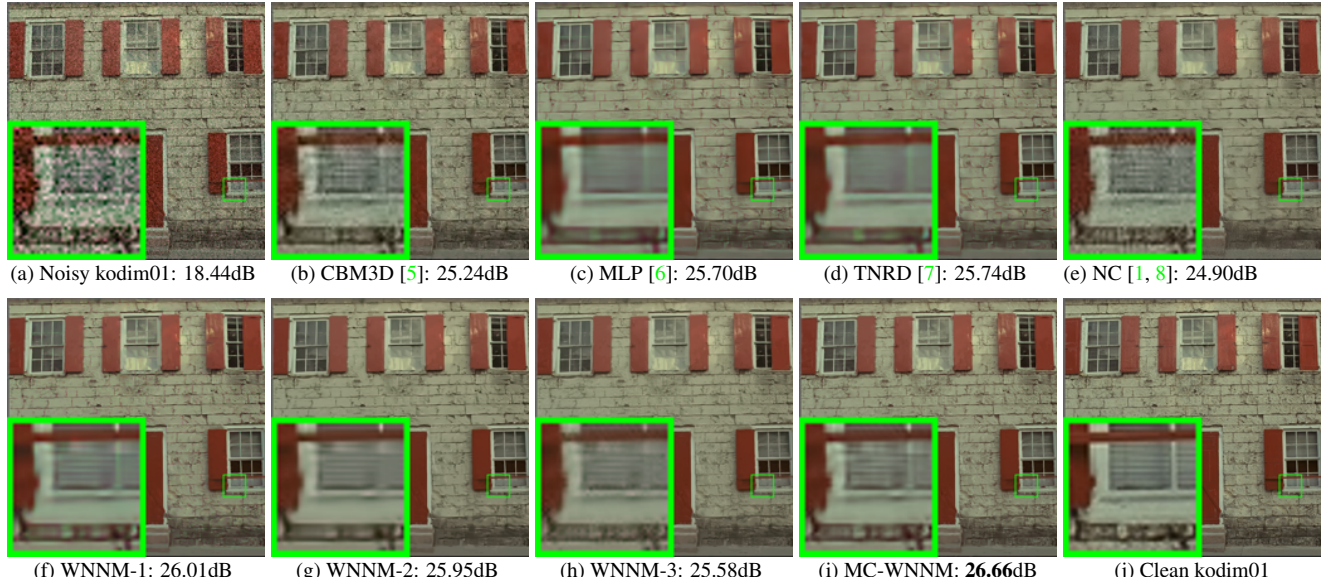
321

322

323

Table 2. PSNR(dB) results of different denoising methods on 24 natural images.

Image#	<b>CBM3D</b>	<b>MLP</b>	<b>TNRD</b>	<b>NI</b>	<b>NC</b>	<b>WNNM-1</b>	<b>WNNM-2</b>	<b>WNNM-3</b>	<b>MC-WNNM</b>
1	23.38	26.49	26.50	24.82	23.59	26.40	25.60	24.76	<b>27.81</b>
2	25.19	30.94	30.90	26.82	27.79	30.89	29.75	29.21	<b>30.96</b>
3	25.39	32.03	32.09	27.52	27.41	32.20	31.17	30.39	<b>32.89</b>
4	24.96	30.55	30.47	27.34	27.00	30.74	29.71	29.10	<b>31.19</b>
5	23.29	26.65	26.73	25.72	26.67	26.74	25.98	24.68	<b>27.60</b>
6	24.09	27.76	27.70	26.10	26.12	27.85	26.96	26.01	<b>29.15</b>
7	24.89	30.70	30.72	27.17	28.07	30.91	29.94	28.87	<b>31.37</b>
8	23.30	26.12	26.27	25.59	26.11	26.87	26.33	24.74	<b>27.44</b>
9	25.20	31.35	31.31	27.74	28.33	31.30	30.45	29.44	<b>32.08</b>
10	25.13	31.01	31.05	27.60	28.53	31.12	30.17	29.21	<b>31.83</b>
11	24.54	28.79	28.82	26.72	24.40	28.73	27.79	26.94	<b>29.60</b>
12	25.43	31.60	31.60	27.82	29.01	31.59	30.62	29.91	<b>32.11</b>
13	22.50	24.71	24.73	24.96	23.36	24.70	23.85	22.86	<b>25.96</b>
14	23.91	27.69	27.72	26.26	23.08	27.62	26.81	25.91	<b>28.57</b>
15	25.45	31.09	31.05	27.36	28.49	31.29	30.21	29.46	<b>31.39</b>
16	24.89	29.79	29.73	27.35	27.10	29.84	28.85	28.13	<b>31.10</b>
17	25.12	30.26	30.24	27.15	27.54	30.11	29.35	28.43	<b>31.08</b>
18	23.83	27.26	27.26	26.05	26.15	27.32	26.18	25.28	<b>28.32</b>
19	24.63	29.40	29.39	27.06	27.41	29.78	28.87	28.05	<b>30.53</b>
20	26.43	31.16	31.27	26.43	26.92	31.25	30.43	29.41	<b>31.55</b>
21	24.24	28.26	28.27	26.66	27.18	28.22	27.45		<b>29.29</b>
22	24.51	29.03	29.06	26.83	27.64	29.02	27.81		<b>29.57</b>
23	25.55	32.87	32.75	27.60	23.75	32.58	31.46		<b>32.34</b>
24	23.85	27.06	27.13	25.86	27.05	27.50	26.63		<b>28.32</b>
<b>Average</b>	24.57	29.27	29.28	26.69	26.61	29.36	28.43		<b>30.09</b>

Figure 1. Denoised images of different methods on the image "kodim01" degraded by AWGN with different standard deviations of  $\sigma_r = 40$ ,  $\sigma_g = 20$ ,  $\sigma_b = 30$  on R, G, B channels, respectively. The images are better to be zoomed in on screen.

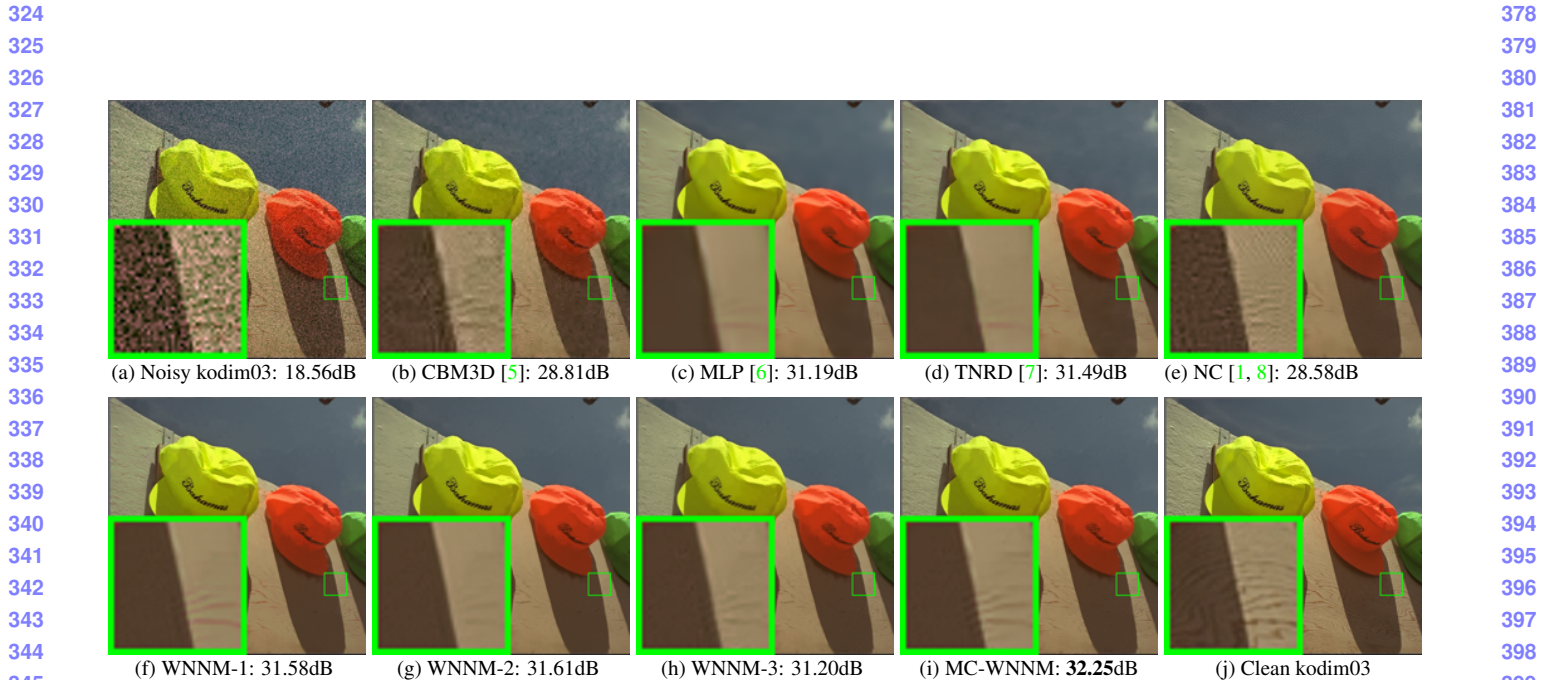


Figure 2. Denoised images of different methods on the image “kodim03” degraded by AWGN with different standard deviations of  $\sigma_r = 40$ ,  $\sigma_g = 20$ ,  $\sigma_b = 30$  on R, G, B channels, respectively. The images are better to be zoomed in on screen.

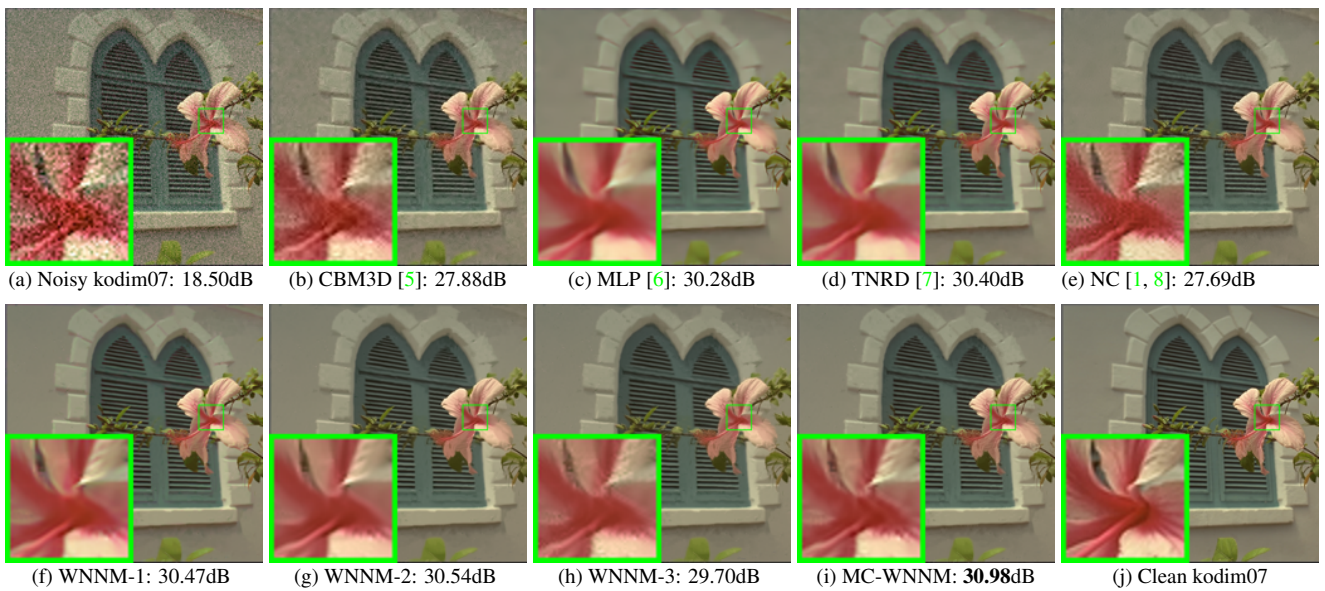


Figure 3. Denoised images of different methods on the image “kodim07” degraded by AWGN with different standard deviations of  $\sigma_r = 40$ ,  $\sigma_g = 20$ ,  $\sigma_b = 30$  on R, G, B channels, respectively. The images are better to be zoomed in on screen.

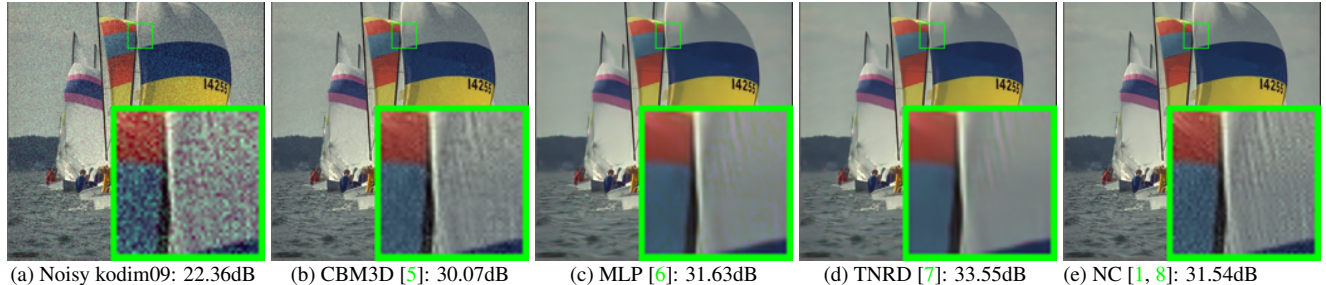
432  
433  
434486  
487  
488444  
445  
446  
447  
448  
449  
450  
451  
452497  
498  
499  
500  
501  
502  
503  
504  
505  
506

Figure 4. Denoised images of different methods on the image “kodim09” degraded by AWGN with different standard deviations of  $\sigma_r = 5$ ,  $\sigma_g = 30$ ,  $\sigma_b = 15$  on R, G, B channels, respectively. The images are better to be zoomed in on screen.

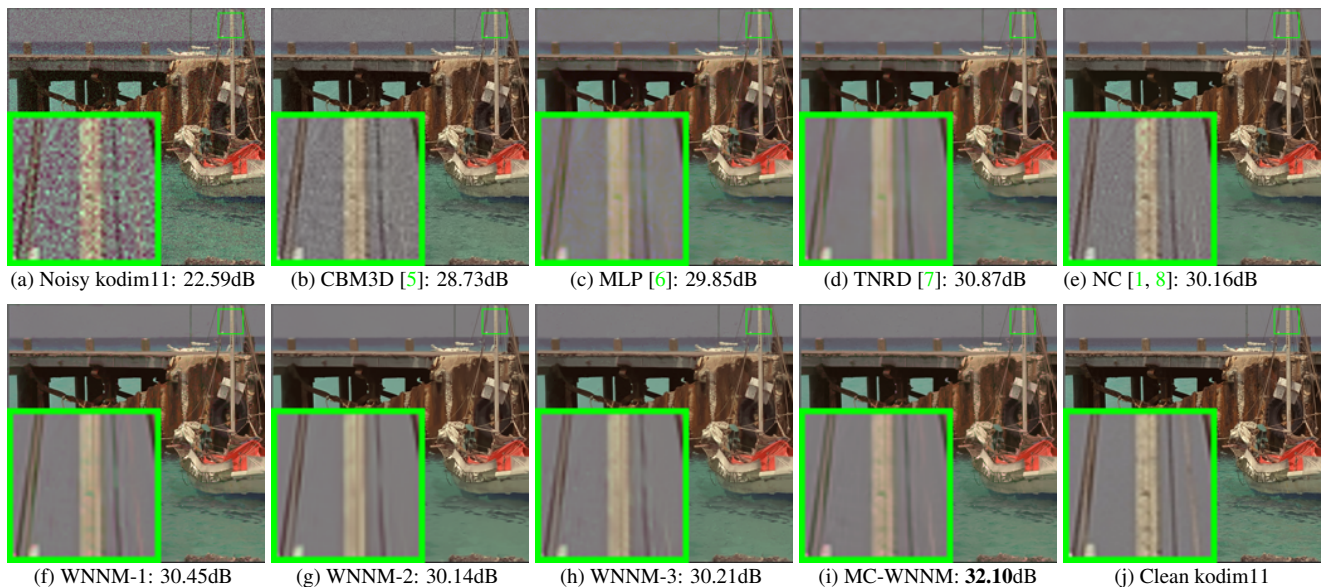
453  
454  
455507  
508  
509456  
457  
458  
459  
460  
461510  
511  
512  
513  
514  
515

Figure 5. Denoised images of different methods on the image “kodim11” degraded by AWGN with different standard deviations of  $\sigma_r = 5$ ,  $\sigma_g = 30$ ,  $\sigma_b = 15$  on R, G, B channels, respectively. The images are better to be zoomed in on screen.

482

535

483

536

484

537

485

538

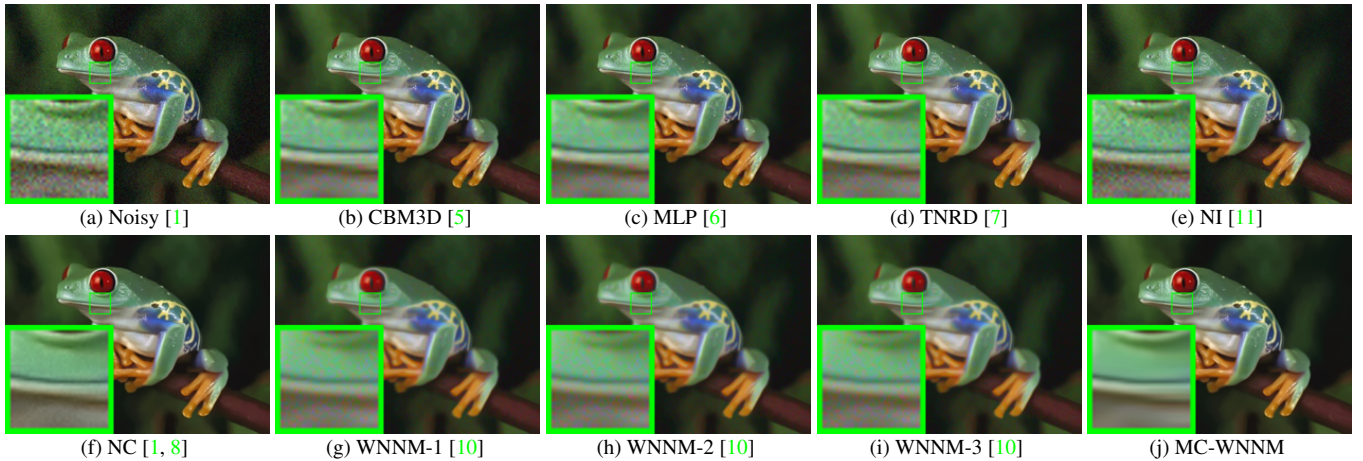


Figure 6. Denoised images of the real noisy image “Frog” [1] by different methods. The images are better to be zoomed in on screen.

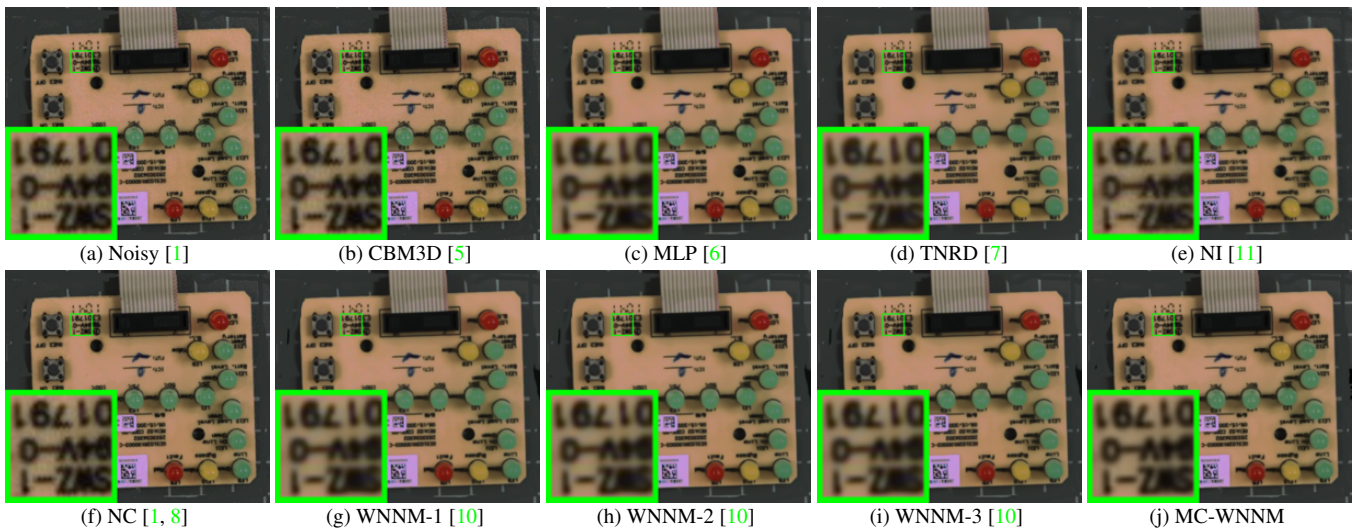


Figure 7. Denoised images of the real noisy image “Circuit” [1] by different methods. The images are better to be zoomed in on screen.

### 3. More visual comparisons of denoised images by different methods on the real noisy images of the dataset [1]

In this section, we give more comparisons of the state-of-the-art denoising methods on the dataset [1]. The real noisy images in dataset [1] have no “ground truth” images and hence we only compare the visual quality of the denoised images by different methods. As can be seen from Figures ??-??, our proposed method performs better than the competing methods.

### 4. More visual comparisons of denoised images by different methods on the real noisy images of the dataset [2]

In this section, we provide more comparisons of the proposed method with the state-of-the-art denoising methods on the 15 cropped real noisy images used in [2]. In this dataset, each scene was shot 500 times under the same camera and camera setting. The mean image of the 500 shots is roughly taken as the “ground truth”, with which the PSNR can be computed. As can be seen from Figures 14-??, in most cases, our proposed method achieves better performance than the the competing methods. This validates the effectiveness of our proposed external prior guided internal prior learning framework for real noisy image denoising.

648  
649  
650  
651  
652  
653702  
703  
704  
705  
706  
707  
708  
709  
710  
711  
712  
713  
714

(a) Noisy [1] (b) CBM3D [5] (c) MLP [6] (d) TNRD [7] (e) NI [11]

(f) NC [1, 8] (g) WNNM-1 [10] (h) WNNM-2 [10] (i) WNNM-3 [10] (j) MC-WNNM

654  
655  
656  
657  
658  
659  
660  
661  
662  
663  
664  
665  
666  
667  
668  
669  
670  
671  
672  
673  
674  
675  
676  
677  
678  
679  
680  
681  
682  
683  
684  
685  
686  
687  
688  
689  
690  
691  
692  
693  
694  
695  
696  
697  
698  
699  
700  
701715  
716  
717  
718  
719  
720  
721  
722  
723  
724  
725  
726  
727  
728  
729  
730  
731  
732  
733  
734  
735  
736  
737  
738  
739  
740  
741  
742  
743  
744  
745  
746  
747  
748  
749  
750  
751  
752  
753  
754  
755

(a) Noisy [1] (b) CBM3D [5] (c) MLP [6] (d) TNRD [7] (e) NI [11]

(f) NC [1, 8] (g) WNNM-1 [10] (h) WNNM-2 [10] (i) WNNM-3 [10] (j) MC-WNNM

Figure 8. Denoised images of the real noisy image “Woman” [1] by different methods. The images are better to be zoomed in on screen.

756  
757  
758  
759

(a) Noisy [2]: 33.88dB (b) CBM3D [5, 9]: 36.40dB (c) TNRD [7]: 36.47dB (d) NI [11]: 34.03dB (e) NC [1, 8]: 34.35dB

(f) CC [2]: 35.37dB (g) WNNM-2 [10]: 35.12dB (h) WNNM-3 [10]: 36.65dB (i) MC-WNNM: 37.28dB (j) Mean Image [2]

Figure 10. Denoised images of a region cropped from the real noisy image “Canon 5D Mark 3 ISO 3200 2” [2] by different methods. The images are better to be zoomed in on screen.

768

769  
770  
771  
772  
773  
774  
775  
776

(a) Noisy [2]: 33.77dB (b) CBM3D [5, 9]: 35.07dB (c) TNRD [7]: 36.37dB (d) NI [11]: 35.16dB (e) NC [1, 8]: 35.34dB

(f) CC [2]: 35.95dB (g) WNNM-2 [10]: 36.42dB (h) WNNM-3 [10]: 36.84dB (i) MC-WNNM: 37.02dB (j) Mean Image [2]

Figure 11. Denoised images of a region cropped from the real noisy image “Nikon D600 ISO 3200 2” [2] by different methods. The images are better to be zoomed in on screen.

807  
808  
809810  
811  
812  
813  
814  
815  
816  
817  
818  
819  
820  
821  
822823  
824  
825  
826  
827  
828  
829  
830831  
832  
833  
834  
835  
836  
837  
838  
839  
840841  
842  
843  
844  
845  
846  
847  
848  
849850  
851  
852  
853  
854  
855  
856  
857  
858  
859  
860  
861  
862  
863

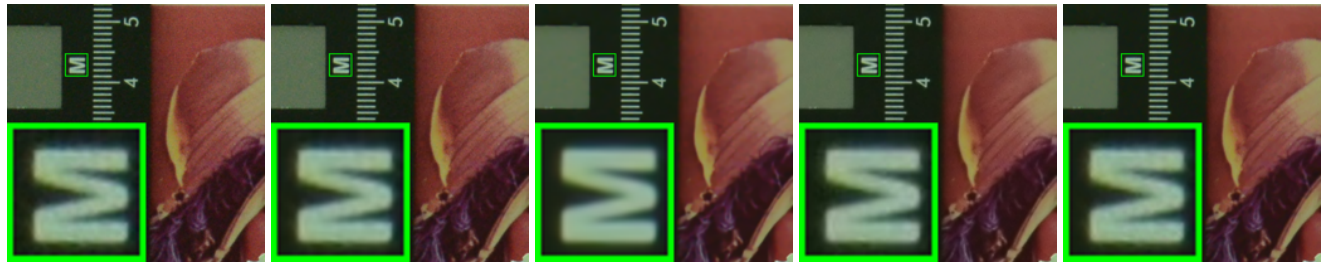
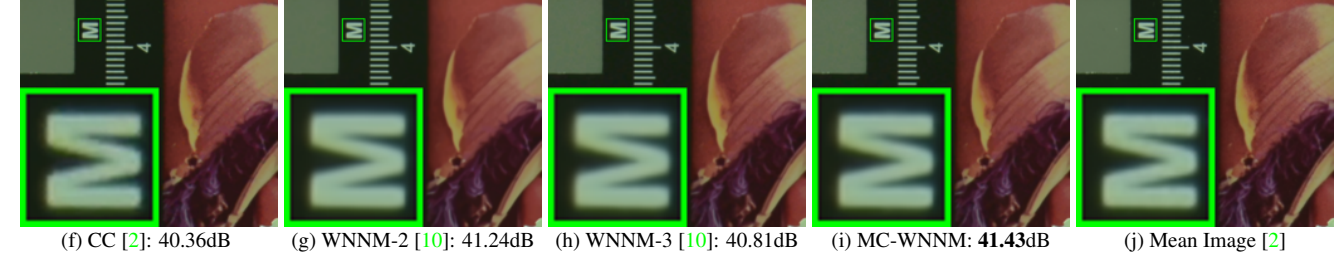
864  
865  
866  
867918  
919  
920  
921872  
873  
874  
875925  
926  
927  
928886  
887931  
932  
933  
934

Figure 12. Denoised images of a region cropped from the real noisy image “Nikon D800 ISO 1600 2” [2] by different methods. The images are better to be zoomed in on screen.

888

940

889  
890  
891  
892  
893  
894941  
942  
943  
944  
945  
946  
947  
948

903

949  
950  
951  
952  
953  
954  
955  
956904  
905  
906  
907  
908  
909  
910  
911957  
958  
959  
960  
961  
962  
963  
964912  
913  
914965  
966  
967

Figure 13. Denoised images of a region cropped from the real noisy image “Nikon D800 ISO 3200 2” [2] by different methods. The images are better to be zoomed in on screen.

915

968

916  
917969  
970  
971

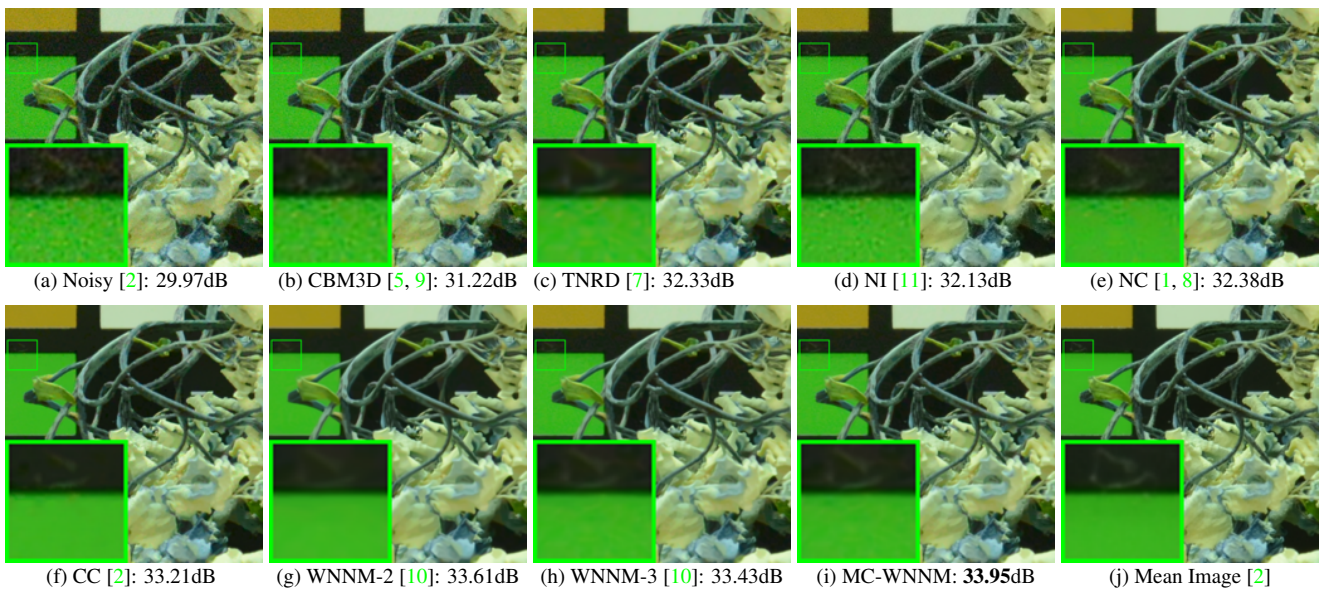
972  
973  
974  
975  
976  
977  
978  
979  
980  
981  
982  
983  
984  
985  
986  
987  
9881026  
1027  
1028  
1029  
1030  
1031  
1032  
1033  
1034  
1035  
1036  
1037  
1038  
1039  
1040  
1041  
1042  
1043  
1044  
1045  
1046  
1047  
1048  
1049  
1050  
1051  
1052  
1053  
1054  
1055  
1056  
1057  
1058  
1059  
1060  
1061  
1062  
1063  
1064  
1065  
1066  
1067  
1068  
1069  
1070  
1071  
1072  
1073  
1074  
1075  
1076  
1077  
1078  
1079

Figure 14. Denoised images of a region cropped from the real noisy image “Nikon D800 ISO 6400 2” [2] by different methods. The images are better to be zoomed in on screen.

1010  
1011  
1012  
1013  
1014  
1015  
1016  
1017  
1018  
1019  
1020  
1021  
1022  
1023  
1024  
1025

1080	<b>References</b>	1134
1081		1135
1082	[1] M. Lebrun, M. Colom, and J. M. Morel. The noise clinic: a blind image denoising algorithm. <a href="http://www.ipol.im/pub/art/2015/125/">http://www.ipol.im/pub/ art/2015/125/</a> . Accessed 01 28, 2015. 1, 3, 4, 5, 6, 7, 8, 9, 10	1136
1083		1137
1084	[2] S. Nam, Y. Hwang, Y. Matsushita, and S. J. Kim. A holistic approach to cross-channel image noise modeling and its application to image denoising. <i>IEEE Conference on Computer Vision and Pattern Recognition (CVPR)</i> , pages 1683–1691, 2016. 1, 6, 8, 9, 10	1138
1085		1139
1086	[3] C. Eckart and G. Young. The approximation of one matrix by another of lower rank. <i>Psychometrika</i> , 1(3):211–218, 1936. 1	1140
1087		1141
1088	[4] S. Gu, Q. Xie, D. Meng, W. Zuo, X. Feng, and L. Zhang. Weighted nuclear norm minimization and its applications to low level vision. <i>International Journal of Computer Vision</i> , pages 1–26, 2016. 1	1142
1089		1143
1090	[5] K. Dabov, A. Foi, V. Katkovnik, and K. Egiazarian. Color image denoising via sparse 3D collaborative filtering with grouping constraint in luminance-chrominance space. <i>IEEE International Conference on Image Processing (ICIP)</i> , pages 313–316, 2007. 3, 4, 5, 6, 7, 8, 9, 10	1144
1091		1145
1092	[6] H. C. Burger, C. J. Schuler, and S. Harmeling. Image denoising: Can plain neural networks compete with BM3D? <i>IEEE Conference on Computer Vision and Pattern Recognition (CVPR)</i> , pages 2392–2399, 2012. 3, 4, 5, 6, 7	1146
1093		1147
1094	[7] Y. Chen, W. Yu, and T. Pock. On learning optimized reaction diffusion processes for effective image restoration. <i>IEEE Conference on Computer Vision and Pattern Recognition (CVPR)</i> , pages 5261–5269, 2015. 3, 4, 5, 6, 7, 8, 9, 10	1148
1095		1149
1096	[8] M. Lebrun, M. Colom, and J.-M. Morel. Multiscale image blind denoising. <i>IEEE Transactions on Image Processing</i> , 24(10):3149– 3161, 2015. 3, 4, 5, 6, 7, 8, 9, 10	1150
1097		1151
1098	[9] K. Dabov, A. Foi, V. Katkovnik, and K. Egiazarian. Image denoising by sparse 3-D transform-domain collaborative filtering. <i>IEEE Transactions on Image Processing</i> , 16(8):2080–2095, 2007. 8, 9, 10	1152
1099		1153
1100	[10] S. Gu, L. Zhang, W. Zuo, and X. Feng. Weighted nuclear norm minimization with application to image denoising. <i>IEEE Conference on Computer Vision and Pattern Recognition (CVPR)</i> , pages 2862–2869, 2014. 6, 7, 8, 9, 10	1154
1101		1155
1102	[11] Neatlab ABSoft. Neat Image. <a href="https://ni.neatvideo.com/home">https://ni.neatvideo.com/home</a> . 6, 7, 8, 9, 10	1156
1103		1157
1104		1158
1105		1159
1106		1160
1107		1161
1108		1162
1109		1163
1110		1164
1111		1165
1112		1166
1113		1167
1114		1168
1115		1169
1116		1170
1117		1171
1118		1172
1119		1173
1120		1174
1121		1175
1122		1176
1123		1177
1124		1178
1125		1179
1126		1180
1127		1181
1128		1182
1129		1183
1130		1184
1131		1185
1132		1186
1133		1187